Scripta METALLURGICA Vol. 16, pp. 203-208, 1982 Pergamon Press Ltd.
Printed in the U.S.A. All rights reserved

T-P PHASE DIAGRAM OF THE Fe-H SYSTEM AT TEMPERATURES TO 450°C AND PRESSURES TO 6.7 GPa

V.E.Antonov, I.T.Belash, and E.G.Ponyatovsky
Institute of Solid State Physics, USSR Academy of Sciences
142432 Chernogolovka, Moscow distr., USSR

(Received November 30, 1981)

Introduction

At T = 250°C and $P_{H_2} \approx 4.5$ GPa a phase transformation occurs in iron followed by a jump-like increase in the hydrogen solubility (1). The hydrogen content in the Fe-H samples obtained by quenching down to -180°C after hydrogenation for 10 h at P_{H_2} = 6.7 GPa and T = 250°C reached the H-to-metal atomic ratio $n \approx 0.8$. The atmospheric pressure investigations have shown that the hydride thus synthesized has an h.c.p. iron sublattice with the parameters a = (.2686 ± .0003)nm, c = (.4380 ± .0005)nm, c/a = 1.631 ± 0.003 at T = -190°C (1) and is a ferromagnetic with the Curie point $T_c \gg 80$ K and spontaneous magnetization $\sigma_0 \approx 2.2\ \mu_B$/Fe atom at T = 0 K (2), where μ_B is the Bohr magneton. At atmospheric pressure and $T \gtrsim -120°C$ iron hydride desintegrates into the metal and molecular hydrogen.

In the present work the T-P_{H_2} phase diagram is developed for the Fe-H system via the measurements of baric and temperature dependences of electrical resistance, R, and initial magnetic permeability, μ_0. For samples we used 0.2 mm dia iron wire purified by zone melting followed by refining in hydrogen at T = 870°C for 100 h (the content of impurities and details of the purification technique are given in (3)). Hydrogen compression was done in "Toroid"-type chambers by the technique suggested in (4). For pressure calibration of the chambers we used the method described in (5). The pressure was measured with an accuracy ±0.3 GPa, the baric hysteresis of phase transformations was determined with an accuracy ±0.15 GPa. The temperature was measured with a chromel-alumel thermocouple insulated against the exposure to hydrogen; the measurement error did not exceed ±15°C. During the process of measuring the temperature was kept constant within ±2°C. The pressure effect on the thermocouple readings was neglected.

Due to the diffusion nature of the formation of the Fe-H solid solutions in the hydrogen atmosphere experiments there occurred temporal drifts, $R(\tau)$ and $\mu_0(\tau)$, at fixed values of T and P_{H_2} after changing pressure or temperature in the intervals of phase transitions as well as in single-phase regions. So, the measurements were carried out in a process of step-wise changes in pressure or temperature; in every point the sample was exposed up to the end of the temporal drift of the measured quantity, and its final value was plotted on the graph.

Results and discussion

The location of anomalies of baric and temperature dependences of R and μ_0 is shown in the T-P_{H_2} phase diagram, Fig.1. One can see that in the temperature and pressure range investigated the lines of phase transformations se-

0036-9748/82/020203-06$03.00/0

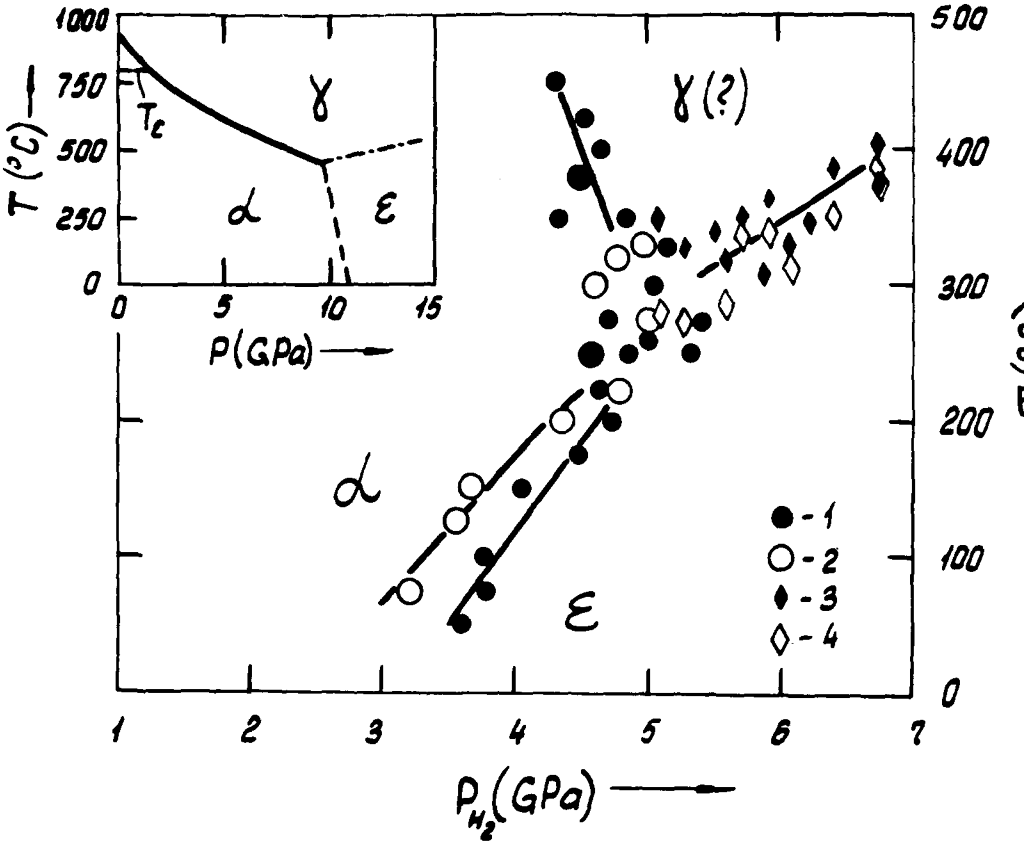

FIG.1

T-P phase diagram of the Fe-H system. 1,2 - location of anomalies on the electrical resistance isotherms (see Fig.3) at increasing and decreasing pressure, respectively; 3,4- location of anomalies on the electrical resistance and initial magnetic permeability isobars (see Fig.4) at heating and cooling, respectively.
In insert - the T-P diagram of iron (7,8); T_c - the Curie points line.

parate the T-P_{H_2} plane into three regions, denoted as α, ε, and γ. The triple-point coordinates are T ~ 280°C, P_{H_2} ~ 5 GPa.

Fig.2a shows the electrical resistance isotherms of iron at T=250°C in an inert medium (petrol) and in hydrogen in the α-phase stability region. In an inert medium the sample resistance decreased monotonously with pressure, no drift, R(τ), occurring after a pressure change. The resistance of the sample immersed in hydrogen atmosphere increased after a pressure change for 10 ÷ 20 min, then reached some limit value and further on was almost constant; while on increasing pressure the R(P_{H_2}) curve deviated still stronger from the R(P) curve in an inert medium. Such a behaviour of the resistance evidences for an increase of hydrogen solubility in the α-phase of the Fe-H solid solution with pressure. An absolute value of this solubility remains, however, rather small and even for samples hydrogenized at P_{H_2} = 4 GPa and T = 250°C does not exceed the sensitivity limit δn ~ 0.01 of the employed method of chemical

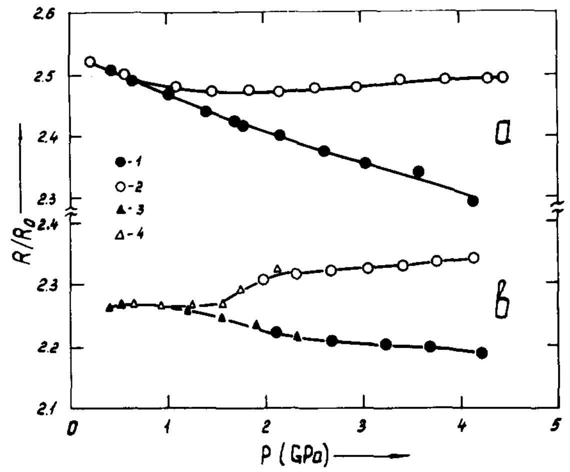

FIG.2

Electrical resistance isotherms at T = 250°C (a - high purity iron, b - carbonyl iron) measured at increasing pressure. 1 - in an inert medium (petrol); 2 - in hydrogen; 3,4 - the same, the data of (9). R_0 is the resistance of the samples at atmospheric pressure and room temperature.

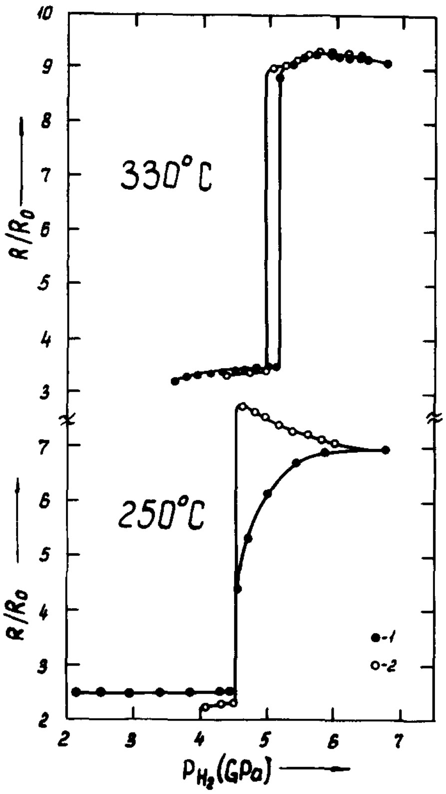

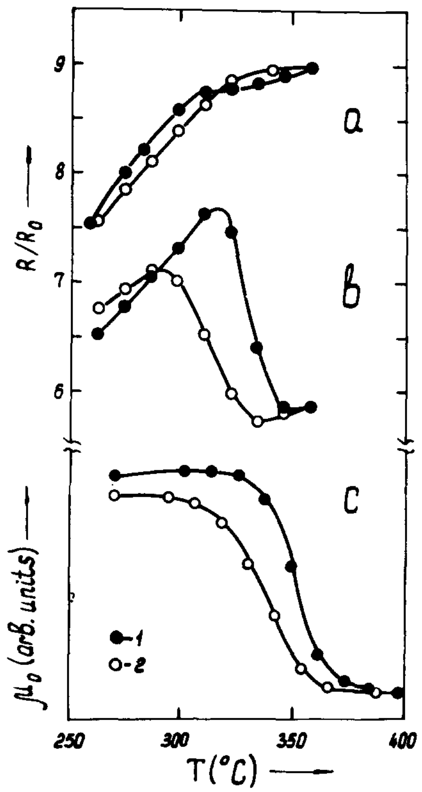

FIG.3. Electroresistance isotherms for iron in hydrogen atmosphere. 1 - at increasing pressure; 2 - at decreasing. R_0 as in Fig.2.

FIG.4. Isobars of the temperature dependences of electroresistance (a,b; P_{H_2} = 6.1 GPa) and initial magnetic permeability (c; P_{H_2} = 5.7 GPa) in the vicinity of the $\varepsilon \rightleftarrows \gamma$ transformation in the Fe-H system. 1 - at heating; 2 - at cooling; a - first cycle of heating and cooling; b - fifth cycle; c - fourth cycle. R_0 as in Fig.2.

analysis (the analysis technique is described elsewhere (1)). It is reasonable to consider the α-phase to be a low-concentrated hydrogen interstitial solution on the base of the b.c.c. iron (at atmospheric pressure iron has a b.c.c. structure at $T \leqq 912^{\circ}C$).

The isotherm of the iron electroresistance measured to $P_{H_2} = 6.7$ GPa in hydrogen atmosphere at $T = 250^{\circ}C$ is shown in Fig.3. The $\alpha \rightarrow \varepsilon$ transition occurring at $P_{H_2} \approx 4.5$ GPa is followed by a jump-like increase in the sample resistance. Here, the resistance drift goes on ~1 h. A pressure increase in the region of the ε-phase stability gives rise to a further growth of the resistance, the characteristic times of saturation of the $R(\tau)$ dependences at fixed P_{H_2}-values gradually decreasing to ~10 min at $P_{H_2} = 6.7$ GPa. A pressure decrease in the region of stability of the ε-hydride causes a further resistance growth, the $R(\tau)$ dependences appearing after a hydrogen pressure change being saturated in $5 \div 10$ min. At $P_{H_2} \approx 4.5$ GPa the hydride decomposes, the process going on for ~1 h, and the sample resistance recovers approximately the same value as that before the hydride formation. A similar behaviour of the $R(P_{H_2})$ dependences is observed at lower temperatures, but the characteristic time intervals needed for the resistance to attain the equilibrium, at given T and P_{H_2} values increase rapidly, and at $T \lessapprox 75^{\circ}C$ they amount to tens of hours. As one can see from Fig.1, at $T \approx 75^{\circ}C$ the $\alpha \rightleftarrows \varepsilon$ transformation possesses a clear hysteresis of ~0.6 GPa. While increasing temperature this hysteresis diminishes, whereas the transformation pressure rises.

Fe-H samples hydrogenized at $T = 250^{\circ}C$ and $P_{H_2} = 6.7$ GPa, i.e. in the region of the ε-phase stability on the T-P_{H_2} phase diagram, have a h.c.p. iron sublattice at $T = -190^{\circ}C$ and atmospheric pressure (1). No other transformation but $\alpha \rightleftarrows \varepsilon$ being observed in the Fe-H system at $T \leq 250^{\circ}C$, it seems logical to consider that the ε-phase forming under high hydrogen pressure is a high-concentrated hydrogen interstitial solid solution (hydride) precisely on the base of a h.c.p. iron sublattice. It is worth noting that the $R(P_{H_2})$ dependences in the vicinity of the $\alpha \rightleftarrows \varepsilon$ transformation in the Fe-H system are analogous to those in the Mo-H system, where the hydride formation is also followed by a b.c.c.→h.c.p. transition in the metallic sublattice (6).

The behaviour of the electroresistance of the Fe-H solid solutions in the vicinity of the $\alpha \rightleftarrows \gamma$ transformation is somewhat different, see Fig.3, isotherm 330°C. While increasing pressure the main change in the resistance occurs at the $\alpha \rightarrow \gamma$ transition. A further pressure increase in the region of stability of the γ-phase results in much smaller changes of R as compared with the case of the ε-phase (Fig.3, isotherm 250°C); the shape of the $R(P_{H_2})$ dependences changes, too. Besides, the γ-phase resistance dependences measured on pressure increase and decrease nearly coincide.

The characteristic time intervals of the resistance drift after a pressure change at $300 \lessapprox T \lessapprox 450^{\circ}C$ amount to $20 \div 40$ min at the $\alpha \rightarrow \gamma$ and $\gamma \rightarrow \alpha$ transitions and several minutes in single-phase regions. The hysteresis of the transformation is within the measurement error $\delta P_{H_2} = \pm 0.15$ GPa. As the temperature rises, the pressure of the $\alpha \rightleftarrows \gamma$ transformation is likely to somewhat decrease (see Fig.1).

Typical resistance isobars for the Fe-H solid solutions in the vicinity of the $\varepsilon \rightleftarrows \gamma$ transformation are shown in Fig.4a,b. At the first cycle of heating and cooling (curve a) the anomalies corresponding to the $\varepsilon \rightarrow \gamma$ and $\gamma \rightarrow \varepsilon$ transitions are not pronounced. After several cycles the amplitude of these anomalies increases considerably (curve b) and at a further thermocycling changes weakly. At P_{H_2} ~5 GPa the resistance drift lasts for ~2 h after a temperature change in the intervals of the $\varepsilon \rightarrow \gamma$ and $\gamma \rightarrow \varepsilon$ transitions and for ~20 min in single-phase regions. At increasing pressure these time intervals reduce, and at $P_{H_2} = 6.7$ GPa they approach ~20 min and ~5 min, respectively. Both the temperatures of the $\varepsilon \rightarrow \gamma$ and $\gamma \rightarrow \varepsilon$ transitions and the hysteresis of the $\varepsilon \rightleftarrows \gamma$ transformation varied strongly from sample to sample and, even, from cycle to cycle at a sequential heating and cooling of the same sample. Nevertheless, the general tendency is as follows: at increasing pressure hysteresis of the $\varepsilon \rightleftarrows \gamma$ transformation decreases, the temperature of the transformation growing (see Fig.1).

A direct investigation of the crystal structure of the γ-phase under high hydrogen pressure has not yet been possible. One is not yet able, either, to fix this state of the Fe-H solution for further studies at atmospheric pressure by means of a rapid cooling of the sample: the electrical resistance measurements have shown that the cooling rate being as fast as ~10°C/s, the $\gamma \rightarrow \varepsilon$ transition does occur, though at a lower temperature than in the case of slow cooling. It is possible, however, to argue in favour of the fact that the γ-phase has to be an interstitial hydrogen solution on the base of a f.c.c. iron sublattice. i) An insert in Fig.1 shows the T-P diagram of iron (7,8), where α, ε, and γ denote the regions of stability of the phases with b.c.c., h.c.p., and f.c.c. structures, respectively. The effect of hydrogen on polymorphous transformations in iron can be estimated from the data for iron alloys with other transition metals whose doping shifts these transformations towards temperature and pressure region convenient for measurements. An investigation of iron-rich Fe-Ni alloys (9) and $Fe_{78}Mn_{22}$ alloy (10) has shown that temperatures of the $\alpha \rightarrow \gamma$ and $\gamma \rightarrow \alpha$ transitions decrease whereas those of the $\varepsilon \rightarrow \gamma$ and $\gamma \rightarrow \varepsilon$ transitions increase in hydrogen atmosphere with respect to their values in an inert medium at the same pressure. It can easily be seen that in case these tendencies are valid for pure iron as well, the $T\text{-}P_{H_2}$ diagram of the Fe-H system must have the same topology as the T-P diagram of iron but with a lower pressure in the triple point ($\alpha + \varepsilon + \gamma$). The experiment yields the diagram of just this type, see Fig.1. ii) All the hydrides of transition metals of VI-VIII groups synthesized by now are hydrogen interstitial solutions on the base of only two closest packings of metal atoms: either h.c.p. (Cr, Mo, Mn, Tc, and Co hydrides) or f.c.c. (Rh, Ni, and Pd hydrides), see (1,11) for references. iii) The $\varepsilon \rightarrow \gamma$ and $\gamma \rightarrow \varepsilon$ transitions in the Fe-H solutions are followed by the electroresistance anomalies (Fig.4) analogous to those observed at the h.c.p. $\rightleftarrows$ f.c.c. transformations in iron (12), Fe-Ru alloys (13), Fe-Mn alloys and hydrogen solutions on their base (10).

Not only the structural, but the magnetic transitions as well can occur in the Fe-H system: at atmospheric pressure α-iron is a ferromagnetic with the Curie point T_c = 769°C (see insert to Fig.1), and ε-hydride of iron is a ferromagnetic with $T_c \gg 80$ K (2). At high pressure it is convenient to fix the magnetic transitions in ferromagnetic substances by controlling the position of the anomalies on the temperature dependence of initial magnetic permeability, μ_0, determined by a differential transformer technique (14). No such anomalies were observed on the $\mu_0(T)$ isobars obtained at temperatures up to 450°C in the region of stability of the α-solutions in the Fe-H system. Therefore, the Fe-H α-solutions remain ferromagnetically ordered in the temperature and pressure range investigated. On the isobars taken at greater hydrogen pressures the anomalies do appear. A typical $\mu_0(T)$ curve is presented in Fig. 4c. Within a possible spread the location of anomalies on the $\mu_0(T)$ dependences coincides with the location of anomalies on the R(T) dependences corresponding to the $\varepsilon \rightarrow \gamma$ and $\gamma \rightarrow \varepsilon$ transitions. The $\mu_0(\tau)$ and $R(\tau)$ drift kinetics is also close here. Thus, one can state that the observed magnetic transformation occurs simultaneously with the structural $\varepsilon \rightleftarrows \gamma$ transformation, and that the ε-phase is ferromagnetically ordered at all temperatures up to that of the $\varepsilon \rightarrow \gamma$ transition throughout the investigated range of hydrogen pressures (to avoid the overload of Fig.1 with superfluous designations we did not mark out in a special way the points of the $\varepsilon \rightarrow \gamma$ and $\gamma \rightarrow \varepsilon$ transitions determined from the measurements of μ_0.

The last problem to be treated here is the effect of the purification degree of initial iron upon the properties of the Fe-H solutions. Measurements have shown (15) that in an inert medium the pressure of the $\alpha \rightarrow \varepsilon$ transition in high purity iron, used in the present work, is, at room temperature, by ~1.5 GPa lower than that in remelted carbonyl iron. It could not be excluded that, depending on the iron purity, the phase boundaries would shift on the $T\text{-}P_{H_2}$ diagram of the Fe-H system as well. To check it up, we have investigated the behaviour of carbonyl iron samples in hydrogen atmosphere. It turned out that within the error limits there occur no shifts of the phase boundaries on the T-P_{H_2} diagram, the only noticeable difference being observed in the electrical resistance behaviour for the α-solutions, see Fig.2. A comparison between isotherms 2a and 2b (T = 250°C) presented in this figure shows that at $P_{H_2} \sim 1.8$ GPa there is a bend on curve 2b for carbonyl iron, that is missing in the case of high purity iron (curve 2a). The causative factors for the appearance of this bend are still obscure. Hydrogen solubility in the α-phase of the Fe-H solid solution on the base of carbonyl iron as well as on the base of high purity iron is not high and does not exceed the sensitivity limit $\delta n \sim 0.01$ of the employed technique of chemical analysis.

Acknowledgements

The authors wish to thank V.I.Shiryaev for the high purity iron samples and K.A.Peresada, A.I.Amelin, and A.N.Grachev for their assistance in conducting the experiment.

References

1. V.E.Antonov, I.T.Belash, E.G.Ponyatovsky, and V.I.Shiryaev, Dokl.Akad.Nauk SSSR 252, 1384 (1980).
2. V.E.Antonov, I.T.Belash, E.G.Ponyatovsky, V.G.Thiessen, and V.I.Shiryaev, Phys.Stat.Sol.(a) 65, K43 (1981).
3. D.S.Kamenetskaya, I.B.Piletskaya, and V.I.Shiryaev, Zhelezo Vysokoi Stepeni Chistoty, Metallurgizdat, Moskva (1978).
4. I.T.Belash and E.G.Ponyatovsky, Patent No. 741105 (USSR).
5. V.E.Antonov, I.T.Belash, Fizika i Tekhnika Vysokikh Davleniy, v.1, p.96, Naukova Dumka, Kiev (1980).
6. V.E.Antonov, I.T.Belash, and E.G.Ponyatovsky, Dokl.Akad.Nauk SSSR 248, 635 (1979).
7. J.F.Cannon, J.Phys.Chem.Ref.Data 3, 781 (1974).
8. E.Yu.Tonkov, Fazovye Diagrammy Elementov pri Vysokom Davlenii, Nauka, Moskva (1979).
9. E.G.Ponyatovsky, V.E.Antonov, and I.T.Belash, Fiz.Metallov i Metallovedenie 44, 1038 (1977).
10. ibid. 46, 1090 (1978).
11. E.G.Ponyatovsky, V.E.Antonov, and I.T.Belash. Izv.Akad.Nauk SSSR, Ser. Neorg.Mater. 14, 1570 (1978).
12. F.P.Bundy, J.Appl.Phys. 36, 616 (1965).
13. L.D.Blackburn, L.Kaufman, and M.Cohen, Acta Met. 13, 533 (1965).
14. G.T.Dubovka and E.G.Ponyatovsky, Fiz.Metallov i Metallovedenie 33, 540 (1972).
15. Yu.A.Litvin, private communication.